Available online at www.dergipark.org.tr/en

INTERNATIONAL ADVANCED RESEARCHES and ENGINEERING JOURNAL

Journal homepage: www.dergipark.org.tr/en/pub/iarej

e-ISSN: 2618-575X

International Open Access

Volume 04
Issue 02

August, 2020

Research Article

Numerical and experimental study on thermal characteristics of louvered fin microchannel air preheaters

Anıl Başaran [a,*] ***and Ali Yurddaş*** [a]

[a]*Manisa Celal Bayar University, Engineering Faculty, Department of Mechanical Engineering, Yunusemre, Manisa, 45140, Turkey*

ARTICLE INFO

Article history:
Received 12 March 2020
Revised 03 May 2020
Accepted 07 May 2020

Keywords:
Microchannel heat exchanger
Microchannel preheater
Numerical modeling
R600a
Thermal characteristics

ABSTRACT

Microchannel heat exchangers have been gradually getting importance in industrial applications due to offering outstanding benefits. The current study has focused on the development of a numerical model to predict the thermal performance of the microchannel air preheaters (MCPH) for HVAC systems. An experimental study has been performed to validate the numerical model results. A louvered fin multiport microchannel heat exchanger has been employed as an air preheater in the experiments. The proposed model has been developed based on the segment-by-segment approach and calculated the outlet temperature and heat capacity of the MCPH. Different air velocities at the frontal face and varying mass flow rates in passes of the MCPH have been taken into consideration in the model. It has been concluded from experimental data that the model predicts the outlet temperature with an average absolute deviation within ±2% for all investigated test conditions. The proposed model shows high accuracy with respect to temperature calculation. Another conclusion is that the non-uniform air velocity approach improves the precision of the proposed model. The heat capacity predictions with the uniform air velocity approach indicate higher deviations than the non-uniform air velocity approach.

1. Introduction

Energy is the one important phenomena for solving the problem requirements in the industry [1]. In this respect, recently, heat transfer requirements from small areas with high heat flux have started to appear with the developing technology. Micro-scale geometries provide some benefits for industrial applications to meet such needs. With the development of micro-manufacturing technologies, various microchannel geometries attracting attention in heat exchangers design for HVAC applications. A compact size-reduced heat exchanger design, improving the total heat transfer coefficient, less air-side pressure drop, and reducing the amount of working fluid are among the outstanding advantages of microchannel heat exchangers [2–4].

Generally, sub-cooling at the outlet of the condenser is desired to guarantee a single phase in the actual application. The main reason for the desiring single-phase of refrigerants at the outlet of the condensers is the effective operation of the system that is based on the VCRC. Sub-cooling is to cool the refrigerant, at uniform pressure and in a liquid state to a temperature which is less than the saturation temperature corresponding to condenser pressure. Sub-cooling improves system efficiency and reduces flash gas production during expansion. Sub-cooling can be carried out in condensers as a single heat exchanger, as well as in secondary heat exchangers such as preheater. Pre-heaters in HVAC applications can make both duties of pre-heating of intake air and sub-cooling of the refrigerant at the same time.

During the design of the thermal systems, the most common problem in terms of designers is not able to estimate the thermal characteristics of the heat exchangers which is a component of the system. The simulation models reliably predict such parameters may offer a considerable contribution to cost-saving, design and optimization efforts thanks to the reduction of the

* Corresponding author. Tel.: +90-236-201-2382.
E-mail addresses: anil.basaran@cbu.edu.tr *(A. Başaran)*, aliyurddas@gmail.com *(A. Yurddaş)*
ORCID: 0000-0003-0651-1453 *(A. Başaran)*, 0000-0002-4683-142X *(A. Yurddaş)*
DOI: 10.35860/iarej.703104

experimental test and cost. Therefore, many researchers have focused on the numerical investigation of heat transfer and fluid flow characteristics inside the microchannels [5–8]. Glazar et al. [9] conducted an experimental and numerical analysis of heat transfer and fluid flow in the compact heat exchanger with different microchannel shapes. They discretized the governing equations using the finite volume method and made a comparison regarding heat transfer effectiveness and pressure drop in single-phase heat transfer. A generalized three dimensional model for microchannel heat exchanger was developed by Ren et al. [10]. Their model uses the port-by-port calculation grid and takes into consideration three-dimensional heat conduction via fins. The governing equations were discretized by using the finite difference method. The model validated by experiments showed the prediction deviations in the heat capacity of the microchannel heat exchangers (evaporator, condenser and gas cooler) within ±5%. Yin et al. [11] studied the mathematical model using the finite element method for a CO_2 gas cooler. The mathematical model was developed for single-phase fluid flow conditions and was verified with the experiments. The segment-by-segment model applied the energy equation with the uniform air-flow assumption. The gas cooler capacity and pressure drop on R 744 side prediction of their model were found agreed with experimental results. An analytical model based on the segmented approach was conducted by Fronk and Garimella [12] for the assessment of the compact gas coolers. They presented the validation of the model with experimental data [13]. For validation of the model, a heat pump facility was used for a water-coupled microchannel gas cooler. It is found that the model estimated the heat duty with an average absolute deviation of 7.5% regard with water and refrigerant inlet conditions. A model to analyze air-cooled compact heat exchangers was developed by Garcia-Casceles et al. [14]. In the model, the authors used cell discretization with R134a and R410A refrigerant and conditions that can be found in HVAC heat exchangers. As a result of the validation, the model is suitable for the designing and sizing of the compact heat exchangers with satisfactory results.

To improve the accuracy of the model, the researchers have taken into account the crucial air-side factors like non-uniform air velocity and temperature. Kim and Bullard [15] were one of the researchers who consider the non-uniform air distribution in their model. They developed and verified a model with the aim of assessing the thermal performance of the microchannel evaporator for R744 mobile air conditioning system. The model based on the finite volume method emphasized the air-side heat and mass transfer process. On the other hand, they outlined the significance of selecting appropriate heat transfer and pressure drop correlation for the refrigerant side according to their simulation results. Yin et al. [16] presented a finite-volume air-cooled microchannel condenser model to evaluate the characteristics of the heat exchanger. They conducted several tests for one-slab and two-slab microchannel heat exchangers on heat transfer and pressure drop. Their model considered maldistribution air velocity and temperature at the front of the microchannel heat exchanger as well as air-side distribution for multi-slabs. Park and Hrnjak [17] carried out an numerical and experimental study on microchannel heat exchanger for an R410A air-conditioning system. The simulation model took into account non-uniform air distribution in front of the microchannel heat exchanger. Simulation and experimental study focused on the air-side hydraulic performance of the louvered fin microchannel automotive heat exchanger was conducted by Liang et al. [18]. In their study, verification with Coil Designer as well experiment was performed with the using of some existing correlations.

Due to environmental impact of Hydrofluorocarbons (HFCs), there are the efforts to find environmental-friendly alternatives of the HCFs. Hydrocarbons (HCs) like isobutane (R600a) are currently under consideration as potential substitutes [19]. Isobutane is one of the widely used refrigerants in the HVAC systems [20]. Although isobutane which is hydrocarbon type refrigerants are flammable and easily ignited, they are widely preferred in air conditioning and refrigeration equipment because of the advantages they offer. The main advantages of isobutane refrigerants may be listed as cheap to produce, non-ozone depletion impact, low contribution to global warming and low toxicity [21,22].

Some experimental and numerical studies have been performed to understand the thermal characteristics of microchannel heat exchangers in the literature. But, reliable and sufficient universal information is lacking especially for isobutane. Most of the studies on air-cooled microchannel heat exchangers have focused on evaporators and condensers in which two-phase refrigerant flow, and relatively few studies have been conducted for microchannel heat exchangers working with single-phase refrigerants such as preheaters. Therefore, the current study aims to provide a contribution to the determination of thermal characteristics of microchannel air preheater for HVAC systems working with isobutane. The finite volume-based model has been numerically applied to predict outlet temperature and heat capacity of the MCPH. The non-uniform air velocity at the frontal face and varying mass flow rates in passes of the MCPH have been taken into consideration in the calculation. The experimental study has been performed using a microchannel pre-heater for the validation of the proposed model.

2. Numerical Modeling

In this study, a louvered microchannel heat exchanger has been modeled as an air preheater. Considered louvered fin microchannel air preheaters (MCPH) is basically composed of inlet and outlet pipes, headers, baffles in headers, flat tubes contain multi-microchannels and louvered fins. A numerical model has been developed with the aim to predict outlet temperature and the heat transfer rate of the MCPH with high accuracy. The considered MCPH can be seen in Figure 1. Test sample MCPH consists of inlet and outlet pipes, right and left-side header, twenty-nine flat tubes and louvered fins between flat tubes. There are baffles in headers to organize the six passes of the test sample MCPH. The first and second passes involve six flat tubes whereas there are five flat tubes in the third and fourth passes. The fifth and sixth passes include four and three tubes, respectively.

The inlet and outlet pipe relate to the right-side header. Refrigerant enters the heat exchanger upper part of the right header and flows out the lower part of the right header after completing the passes. Each flat-tube includes sixteen rectangular and two semi-circular microchannel ports. Detailed schematics of the cross-section of the microchannel flat tubes with geometric parameters of the louvered fin is indicated in Figure 2. The dimensions of the MCPH are given in Table 1.

The proposed model is based on the widely accepted finite volume method and calculation is conducted numerically with an iterative scheme. In the model, there is a need to create finite volumes (in other words grids) for the calculations. The flat tubes have been divided into a certain number of small elements (also called segments) along the refrigerant flow path to achieve low-temperature change in refrigerant in a segment during calculations. Thereby, the refrigerant properties can be assumed to be constant in a segment during calculations. The representation of a calculation segment is given in Figure 3.

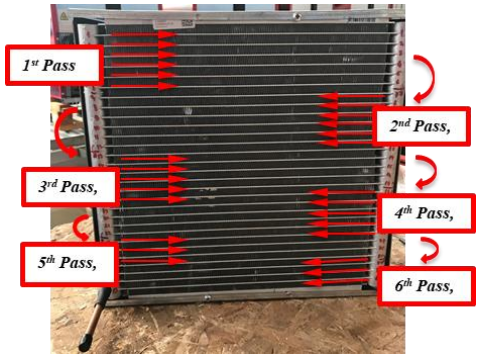

Figure 1. Considered louvered fin microchannel air preheaters (MCPH)

Table 1. Detailed geometrical parameters of the MCPH

Parameters	Dimensions (mm)
Overall structure	
Height, **h**	300.7
Length, **l**	330
Depth, **d**	16.48
Number of the tube, $\mathbf{N_t}$	29
Number of the pass, $\mathbf{N_p}$	6
Pass distribution	6/6/5/5/4/3
Number of port*,$\mathbf{N_{mc}}$	18
Ports (microchannels)	
Height, $\mathbf{P_h}$	0.74
Width, $\mathbf{P_w}$	0.63
Thickness, $\mathbf{P_t}$	0.28
Web thickness, $\mathbf{W_t}$	0.3
Tubes	
Height, $\mathbf{T_h}$	1.3
Width, $\mathbf{T_w}$	16.48
Length, $\mathbf{T_l}$	290
Pitch, $\mathbf{T_p}$	9.4
Fins	
Height, $\mathbf{F_h}$	8.1
Depth, $\mathbf{F_d}$	16
Pitch, $\mathbf{F_p}$	0.55
Thickness, $\boldsymbol{\delta_f}$	0.1
Louvers	
Height,$\mathbf{L_l}$	6.615
Pitch, $\mathbf{L_p}$	1
Angle, $\boldsymbol{\theta}$	18°

* Each tube

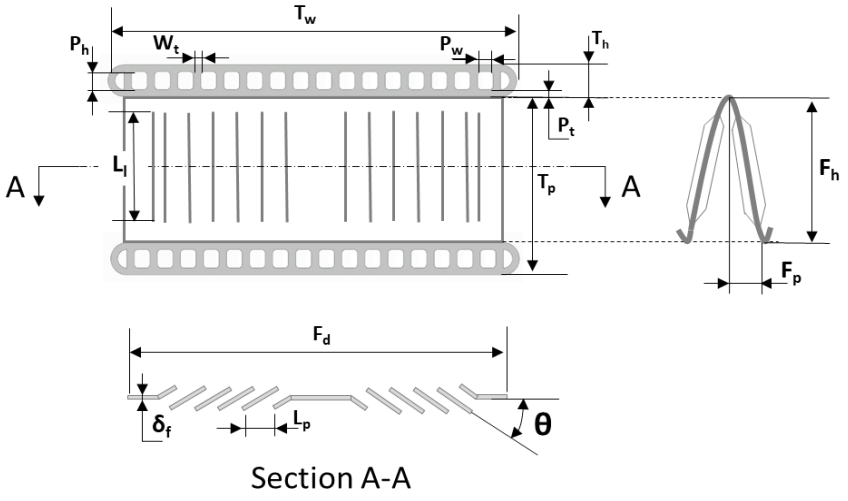

Figure 2. Detailed schematics of the cross-section of the microchannel flat tubes with geometric parameters of the louvered fin

The segments are strictly linked with adjacent segments and thereby a calculation sequence of the segments is created. The outlet conditions of the segments that are calculated with iterative scheme are set inlet conditions of the next segment in the calculation sequence. The calculation sequence of the segments starts at the inlet of the first pass and it is applied in direction of the downstream of the tube.

The solver proceeds to the header which links the following pass of the MCPH. The outlet conditions of the previous header are set as the inlet conditions of the following header (first level of the grid generation). The calculation procedure applied for the segments in next passes in a similar way and it goes on until outlet header. After the solution of all segments, the whole MCPH is simulated to determine thermal characteristics.

The present model suggests that each segment analyzed as an independent cross-flow heat exchanger and the calculation algorithm of the numerical model is applied to each segment for determining thermal characteristics. For all calculation segment, the arithmetic average of the inlet and outlet conditions of the segments are used to evaluate constant refrigerant properties within the segment. The defined refrigerant properties are used to calculate heat duty and pressure drop for that segment. Initially, refrigerant inlet conditions are known, and they are set as the inlet for the first segment. However, firstly, an initial assumption is made due to the fact that the outlet condition cannot be known initially and then an iterative scheme is applied to refine the solution. The iterative scheme is presented in Figure 4.

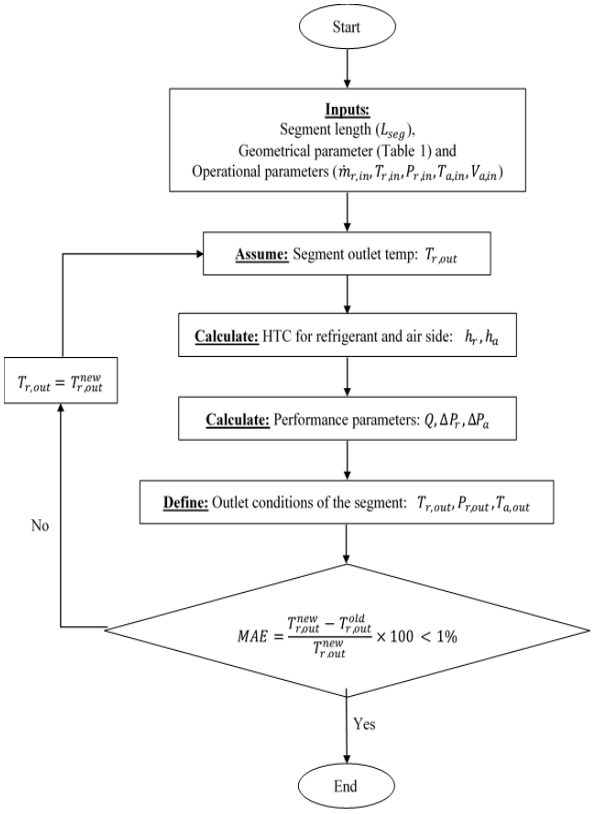

Figure 4. Iterative scheme of the model

The outlet temperature has been considered as a convergence criterion for a segment. In the iteration scheme, convergence criteria between calculated outlet temperatures every iteration have been determined as 1% of Mean Absolute Error (MAE). The MEA for the outlet temperatures of the segment can be calculated by using the following equation:

$$MAE = \frac{T^{new} - T^{old}}{T^{new}} \times 100 \quad (1)$$

The outlet temperature calculated in the previous iteration has been compared with the calculated outlet temperature for that segment. If the MAE percent is lower 1%, iteration is stopped for that segment otherwise iteration proceeds until outlet temperature of the segment converges. After convergence, the iterative calculation is applied next segment in the sequence. It is worth note that initially assumed outlet temperature is used to calculate MAE in the first iteration.

The most of air-cooled heat exchanger applications, the airflow over the heat exchanger is produced by an induced shaft fan. The fan generally is placed in front of the heat exchanger in a canal and it supplies airflow to heat exchangers by means of blowing or pulling off the air. The four walls of this heat exchanger unit give rise to decreasing air velocity near the walls. On the other hand, considering the geometry of the fan blade, the blade connects with a shaft at its middle point and it turns around of this axis. Hence, at this point, the force to blow or pull the air cannot be generated. This configuration of the heat exchanger units causes the non-uniform airflow at the face of the heat exchanger. The proposed model takes into consideration uniform airflow to improve the accuracy of the model. In this content, the model recommends that the face of the MCPH is divided into certain regions to model air-side maldistribution due to fan-driven airflow.

The inputs of the model can be classified into two parts: geometrical inputs and operational inputs. Geometrical inputs cover all principle dimensions of the heat exchanger in both refrigerant and air sides. Geometrical inputs can be listed: height, depth, and length of flat tubes, number of microchannel ports, the dimensions of the microchannels, the fin pitch, length and thickness, the louver angle, pitch, and length. In addition to these parameters, segment length is one of the geometrical inputs of the model. Operational inputs for the model are the mass flow rate of refrigerant, refrigerant inlet temperature and pressure, air velocity distribution and air inlet temperature at the face of each grid region in the second level of grid generation. Refrigerant outlet temperature and heat transfer rate are the output variables of the model.

2.1 Calculation Procedure of the Numerical Model

The suggested numerical model includes the following major assumptions:

- The refrigerant mass flow rate is uniform among the tubes and parallel microchannels in tubes, there is no maldistribution between the microchannels,
- There is one-dimensional refrigerant flow in a segment,
- The air-side velocity in parts created at the second level of discretization are uniform, and air-flow across these parts is independent each other,
- The heat conduction between tubes and are neglected, the center of the fin is considered adiabatic.
- The longitudinal conduction and heat transfer between microchannel are ignored,
- The header is considered as adiabatic and the heat transfer in the header is ignored,
- Refrigerant assumed as well-mixed in headers,
- Both flows in air-side and refrigerant side are considered as steady-state

As stated earlier, each segment is considered as an independent cross-flow heat exchanger and heat transfer between the refrigerant and airflow in a segment is calculated by applying heat exchanger analysis tools. When a segment considered, the Effectiveness-Number of Transfer Units (ε-NTU) method can be applied to calculate heat transfer duty in the segment because of known inlet conditions and unknown outlet conditions initially [23,24]. Meanwhile, the pressure drop of the refrigerant side in the calculation segment is analyzed. As mentioned above, the outlet conditions are calculated by using heat transfer duty and pressure drop and then the iterative scheme is applied. After completed the iterative procedure in each cell, global variables like heat transfer, etc. are calculated by summing all the segment contributions.

In the ε-NTU method, effectiveness is defined for a specified heat exchanger as the ratio of actual heat transfer rate to the maximum possible heat transfer rate [25]:

$$\varepsilon = \frac{\dot{Q}}{\dot{Q}_{max}} \tag{2}$$

Effectiveness is a measure of thermal performance and non-dimensional. The value of the effectiveness ranges from 0 to 1 and it depends on the number of transfer units (NTU), the heat capacity ratio (C_R), and the flow arrangement. In the present study, the mathematical model has been developed for the louvered fin heat exchangers in which both air and refrigerant sides are unmixed. Also, the considered calculation segments have crossflow. Therefore, the effectiveness of a given segment can be calculated by using Eq. (3) for single-phase and Eq. (4) for two- phase refrigerant flow [26].

$$\varepsilon = 1 - exp\{NTU^{0.22}[exp(-C_R NTU^{0.78}) - 1]/C_R\} \tag{3}$$

$$\varepsilon = 1 - \exp(-NTU) \tag{4}$$

where the heat capacity ratio, C_R can be written as follows:

$$C_R = \frac{C_{min}}{C_{max}} = \frac{\min(C_r, C_a)}{\max(C_r, C_a)} \tag{5}$$

where $C_r(= \dot{m}_r C_{p,r})$ and $C_a(= \dot{m}_a C_{p,a})$ are stand for the heat capacity rate of refrigerant and air, respectively. The Number of Transfer Units, NTU designates the non-dimensional heat transfer size or thermal size of the heat exchanger and it is defined as the ratio of overall heat transfer coefficient to the minimum heat capacity rate. NTU can be written as [27]:

$$NTU = \frac{UA}{C_{min}} \tag{6}$$

In the Eq. (7), the maximum possible heat transfer, Q_{max} is expressed as:

$$\dot{Q}_{max} = C_{min}(T_{r,in} - T_{a,in}) \tag{7}$$

Based on the earlier stated assumptions, the heat transfer rate between the streams in each segment by employing the ε-NTU method can be written as follows:

$$\dot{Q} = \varepsilon Q_{max} = \varepsilon C_{min}(T_{r,in} - T_{a,in}) \tag{8}$$

The actual heat transfer rate, Q in a segment may be also written as in Eq. (9) and Eq. (10),

$$\dot{Q} = \dot{m}_r(i_{r,in} - i_{r,out}) \tag{9}$$

$$\dot{Q} = \dot{m}_a(i_{a,out} - i_{a,in}) \tag{10}$$

The overall heat transfer coefficient, UA is the definition of the total thermal resistance to heat transfer between the refrigerant and air.

$$UA = \left[\frac{1}{\eta_o h_a A_a} + \frac{P_t}{k_{tube} A_r} + \frac{1}{h_r A_r}\right]^{-1} \tag{11}$$

According to fin and tube model developed by Singh et al. [28], when the heat conduction between tubes is taken into consideration, predicted heat load is agreement within ±3% of the experimental data whereas there is ±5% agreement when the heat conduction ignored between tubes. Asinari et al. [29] reported that adiabatic-fin tip efficiency which neglects the longitudinal heat conduction in fin gives a reasonably accurate prediction of total heat flow exchanged. They also concluded that the longitudinal and the transverse conduction in tubes, as well as the longitudinal conduction in fin, have negligible impacts on the total heat transfers and on the temperature field. In this context, the assumption of heat conduction only in along fin height direction (one-dimensional heat conduction) can be applied to evaluate the fin efficiency.

Overall fin efficiency which is area-weighted fin efficiency is written as follow:

$$\eta_o = 1 - \frac{A_f}{A_a}(1 - \eta_f) \tag{12}$$

where A_a and A_f are air-side overall heat transfer area and fin surface area, respectively. The fin efficiency is given as:

$$\eta_f = \frac{tanh\,(ml)}{ml} \tag{13}$$

$$m = \sqrt{\frac{2h_a}{k_{fin}\delta}\left(1+\frac{\delta}{F_d}\right)} \tag{14}$$

$$l = \frac{F_h}{2} - \delta \tag{15}$$

In the implementation of the ε-NTU methodology, refrigerant and air-side heat transfer coefficient plays a key role. There is thus need the employment of efficient correlations for the heat transfer coefficient calculation in the model.

2.2 Refrigerant Side Heat Transfer and Pressure Drop

In literature, well-known heat transfer correlations for single-phase are Dittus-Boelter [30], Gnielinski [31] and Perukhov [32]. These correlations have been developed for conventional tubes, but some studies have been conducted to examine the usage of these correlations for microchannels. Derby et al. [33] presented a comparison between single-phase Nusselt numbers obtained by experiments for different cross-sectional microchannels and by Gnielinski [31] correlation. They concluded that single-phase experiments for heat transfer coefficients in the microchannel are within good agreement the Gnielinski [31] correlation. The heat transfer coefficient for single-phase flow in the microchannel can be estimated by the Gnielinski correlation [34]. Gnielinski correlation is

$$Nu_{GN} = \frac{\left(f/8\right)(Re_D - 1000)Pr}{1 + 12.7\sqrt{f/8}\,(Pr^{2/3} - 1)} \tag{16}$$

$$(2300 < Re_D < 10^6)$$

$$Nu_{GN} = 4.36 \quad (Re_D < 2300) \tag{17}$$

where is the friction factor and defined by Filonenko [35] as:

$$f = [1.82\,log(Re_D) - 1.64]^{-2} \tag{18}$$

where Reynolds number is given in below:

$$Re_D = \frac{G_r D_h}{\mu_r} \tag{19}$$

Adams et al. [36] proposed the correction of the Nusselt number for small diameter based on their experimental data. They present the following equation:

$$Nu = Nu_{GN}(1 + F) \tag{20}$$

$$F = CRe_D\left[1 - \left(\frac{D_h}{D_0}\right)^2\right] \tag{21}$$

The constant C and D_0 have been found by using the least-squares fit to all data sets studied by Adams et al. [36] as $C = 7.6\ 10^{-5}$ and $D_0 = 1.164\ mm$.

The refrigerant side pressure drop for single-phase flow may be calculated based on the correlation given in below:

$$\Delta P_r = f\rho_r Um_r^2 \frac{L_{seg}}{2D_h} \tag{22}$$

where Um is the mean velocity of the refrigerant.

2.3 Air-side Heat Transfer Coefficient and Pressure Drop

For microchannel heat exchangers, air-side thermal resistance is dominant over refrigerant-side thermal resistance [37], and thus, understanding of louvered fin performance plays a key role in the prediction of the overall performance of the MCPHs. The numerous studies on the air-side performance of louvered fin heat exchangers have been conducted by many researchers. Among them, widely-used correlations are Chang and Wang [38] correlation and Kim and Bullard [39] correlation. In the suggested model, Chang and Wang [38] correlation is considered in order to calculate the air-side heat transfer coefficient. It is possible that the Chang and Wang correlation with respect to the dimensionless heat transfer coefficient: the Colburn-j factor:

$$j = Re_{LP}^{-0.49}\left(\frac{\theta}{90}\right)^{0.27}\left(\frac{F_p}{L_p}\right)^{-0.14}\left(\frac{F_h}{L_p}\right)^{-0.29}\left(\frac{F_d}{L_p}\right)^{-0.23}\left(\frac{L_l}{L_p}\right)^{0.68}\left(\frac{T_p}{L_p}\right)^{-0.28}\left(\frac{\delta}{L_p}\right)^{-0.05} \tag{23}$$

where Re_{LP} is the Reynolds number depend on louver pitch:

$$Re_{LP} = \frac{\rho_a Um_a L_p}{\mu_a} = \frac{G_a L_p}{\mu_a} \tag{24}$$

It is worth note that the above correlation is valid in Reynolds number range from 100 to 3000. When the Colburn-j factor is found, the air-side heat transfer coefficient can be determined as follow:

$$h_a = j\rho_a Um_a Cp_a {Pr_a}^{-2/3} \tag{25}$$

Another well-known correlation Kim and Bullard [39] is used to calculate the air-side pressure drop. Kim and Bullard friction factor correlation is given in below:

$$f_a = Re_{LP}^{-0.781}\left(\frac{\theta}{90}\right)^{0.444}\left(\frac{F_p}{L_p}\right)^{-1.682}\left(\frac{F_h}{L_p}\right)^{-1.22}\left(\frac{F_d}{L_p}\right)^{0.818}\left(\frac{L_l}{L_p}\right)^{1.97} \tag{26}$$

$$\Delta P_a = f_a {G_a}^2 \frac{F_d}{2\rho_a L_p} \tag{27}$$

3. Experimental Study

A louvered fin microchannel heat exchanger has been tested in order to evaluate the model results. The validation approach of the proposed model against experimental data is employed in this section.

For validation of the model, MCPH tests have been conducted within a vapor compression refrigerant cycle (VCRC). Due to the fact that the VCRC has been used in

many application fields for many years, the equipment with low uncertainties has been developed for the VCRC. Besides, the setup and operation of the VCRC have become easy over the years. All tests have been conducted in a climatic chamber in order to keep constant air properties. The schematics of the test facility and location of the measurement instrumentations can be seen in Figure 5. The MCPH sample has been installed in a small channel with the fan, which supplies air-flow over louvered fins. The test sample heat exchanger has been installed next to the condenser as an air preheater. Thanks to this configuration, a slight increment in temperature of intake air and sub-cooling in after refrigerant can be provided.

The refrigerant flows through the closed-loop the VCRC and a coriolis type flow meter employed in the test facility to measure the refrigerant mass flow rate. The Coriolis flowmeter has an accuracy of less than 0.1% of the rate from -50 to 180 ºC temperature until a maximum 410 bar pressure. The temperature at the inlets and outlets of each component of the VCRC were measured to screen the thermodynamic cycle. Temperature measurements were taken from many points on the heat exchanger, which is the focus of this study. The refrigerant temperature was measured at the inlet and outlet of every two flat tubes on the MCPH as well as the MCPH inlet and outlet. The temperature measurements were used to determine the temperature distribution on the MCPH. The temperature measurements were carried out by means of the T-type thermocouples with measurement sensitivity up to 0.02 ºC in the range of -200 to 400 ºC. Besides temperature measurements, low- and high-pressure measurements on the cycle were conducted. The piezoresistive pressure transmitters with an accuracy ±0.25% FS in the range 2/30 bar were installed for pressure measurements.

Owing to the configuration of the installation of MCPH and supplying the air-flow over the MCPH by an induced-draft-fan, the face of MCPH divided into nine regions in both x and y-direction. As stated earlier, the main purpose of this grid generation, which is characterful of the proposed model, is to take into consideration the effect of the air-side maldistribution. Hence, air-side measurements were conducted at the mid-point of these nine air-side regions. The air-side measurement regions can be seen in Figure 6. The air velocities at air-side regions were measured by using hot-wire anemometer with a resolution 0.01 m/s and an accuracy ±0.1 m/s in 0 to 30 m/s measuring range. Although the air temperature and relative humidity were kept constant in the climatic chamber, their values were checked with their measurements conducted at nine air-side measurement regions with thermo-hygrometer. The thermo-hygrometer has -20 to 60 ºC measuring range, ±0.5 ºC accuracy for temperature measurements and 0 to 100%rH, ±1.8%rH accuracy for relative humidity measurements. Also, the dew point and wet bulb temperature of the air calculated to control the occurrence of wet conditions on the fins.

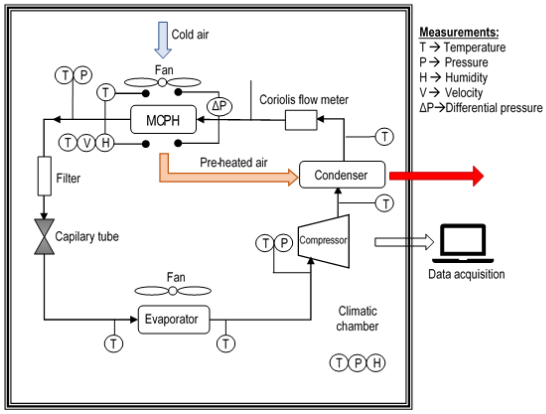

Figure 5. Schematic representation of the test facility

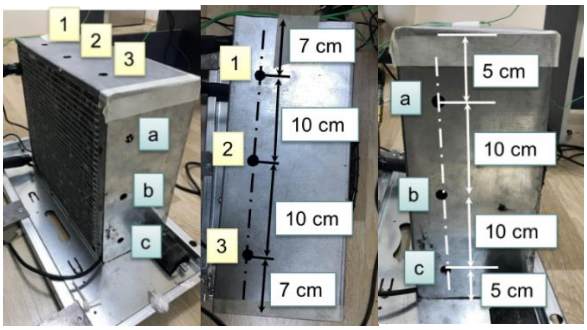

Figure 6. Air-side measurements points

For the verification, experimental measurements were used as the operational inputs of the model in addition to geometrical inputs (Table 1). Iterative scheme and calculation procedure of the model was performed using EES [40]. The outputs variables calculated by using the model have been verified with the output variables obtained from experiments.

The deviations in heat capacity predictions are higher than the ones in the outlet temperature of the MCPH. The main reason for these deviations is more probably to neglected heat transfer in the headers. The model assumes no heat transfer in the header and applies the temperature of the header as the inlet temperature of the next pass. However, in the actual process, there is a slight heat transfer in the header during refrigerant flows from a pass to another. Due to this heat loss, the temperature of the refrigerant decreases a little bit when it changes the passes. Also, it is apparent that the model with non-uniform air velocities overestimates the heat capacity according to experimental results. These overestimated results could have been caused by the heat losses in the header in experiments. Another proof explains this situation can be seen in Table 4. Table 4 exhibits the mean absolute errors between experimental and calculated temperatures at the inlet and outlet of each pass under test conditions. In Table 4, the mean absolute errors at the first pass inlet are equal to zero because experiment measurements at the inlet were applied as inlet conditions in the model. Therefore, in experiments and model calculations, there are the same temperatures in the first part of inlets. It is

obviously seen that the mean absolute errors for temperature in most of the data points have negative value because of the temperature decrease resulted in heat loss in headers. In Table 4, the mean absolute errors at the inlets are higher than the ones at outlets. When the refrigerant flows in the next pass, the model assumes there are no changes in refrigerant temperature between previous and next pass whereas there is a slight temperature decrease in actual operation due to heat losses in the header. Hence, the higher mean absolute errors can be observed at the inlets of the passes. However, these errors have not exceeded 16%. The overall average errors are within the -7 and 2% in terms of the inlet and outlet temperatures of the passes for all tests. Therefore, it can be concluded that the proposed model presents the results with acceptable precisions.

4. Results and Discussion

The present model verification was conducted with a comparison between model and experiment results. Table 2 indicates the refrigerant side test conditions at each data point used to validate model predictions. Air-side test operational conditions for the test are given in Table 3. It is worth note that the air-side parameters were kept constant for test conditions thanks to the climatic chamber. The assessment of the outlet temperature of the MCPH is indicated in Figure 7. It follows from Figure 7 that the proposed model reasonably estimated the outlet temperature of the MCPH. The mean absolute errors for the outlet temperature of the MCPH are in the range ±2%. The model has 2.19% maximum and 0.26% minimum deviation in the MAE for the outlet temperature of the MCPH. It is easily seen from Figure 7 that the model mostly under-estimate the outlet temperature of the MCPH. But, the great majority of the data points show a slightly low error percent. The results show that the proposed numerical model in the current study has high accuracy with respect to the outlet temperature of the MCPH.

Figure 8 exhibits the comparisons of heat capacities of the MCPH obtained experiments and models with both non-uniform and uniform air velocity approaches. In the non-uniform approach, different air velocity applied at the mid-point of the nine air-side grid regions which were created at the second level of the grid generation, while the average air velocity was uniformly applied to the face of the MCPH in the uniform air velocity approach. According to Figure 8, the overall deviation in model results with non-uniform air velocity is within nearly 0 to 20% for the heat capacity of the MCPH. The heat capacity prediction with the uniform air velocity approach indicates the deviations higher than the deviations of the non-uniform air velocity approach. It exceeds the -20% mean absolute error compared with experimental data. It can be easily said that the non-uniform air velocity approach improves the precision of the proposed model. It is obvious that the precision of the model can be increased as the nine air-side regions are augmented.

Under investigated test conditions, the refrigerant enters the MCPH at a temperature in the range 43-49 °C and it is cooled down to nearly 26 °C. Figure 9 demonstrates the refrigerant temperature for investigated test conditions with respect to the length of the refrigerant pass.

Table 2. Test conditions for refrigerant side

Test no	Mass flow rate [g/min]	Inlet temperature [°C]	Inlet Pressure [bar]
1	77	45.02	6.38
2	79	43.16	5.97
3	76	49.61	7.08
4	75	47.43	6.76
5	76	47.70	6.79
6	75	47.77	6.79
7	76	48.00	6.80
8	75	47.4	6.73
9	75	47.71	6.91
10	76	47.46	6.76
11	75	47.08	6.63
12	74	46.67	6.6
13	74	46.83	6.65
14	74	46.35	6.55

Table 3. Test conditions for airside

Location	Inlet Velocity [m/s]
1a	1.6937
2a	1.6383
3a	0.4474
1b	0.4755
2b	0.2011
3b	0.6285
1c	0.6604
2c	1.6765
3c	0.7837

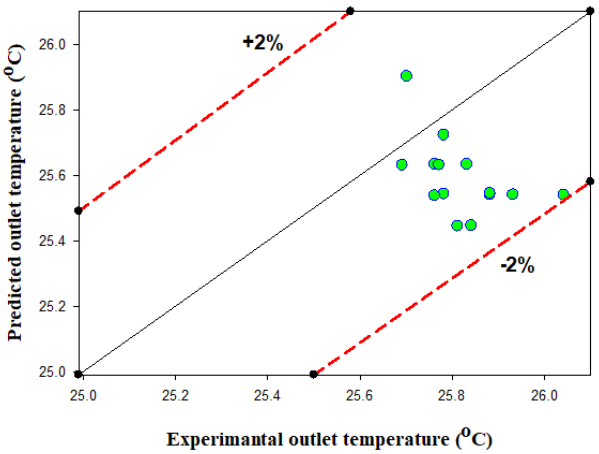

Figure 7. Comparison of the experimental and predicted outlet temperature of the test sample MCPH

Table 4. Mean absolute error between inlet and outlet temperatures of the passes under the test conditions.

		Test 1	Test 2	Test 3	Test 4	Test 5	Test 6	Test 7	Test 8	Test 9	Test 10	Test 11	Test 12	Test 13	Test 14
Pass 1	*Inlet*	0	0	0	0	0	0	0	0	0	0	0	0	0	0
	Outlet	-0.54	3.41	-14.26	-9.91	-9.29	-9.98	-10.32	-8.61	-11.43	-11.53	-12.26	-10.47	-11.73	-10.63
Pass 2	*Inlet*	-1.04	8.33	-16.15	-11.12	-11.53	-12.08	-11.97	-10.77	-15.09	-14.27	-13.93	-12.59	-13.44	-12.36
	Outlet	3.84	2.84	-2.07	0.01	-1.10	-1.28	-0.91	-0.81	-1.67	-1.82	-2.15	-1.53	-2.10	-1.68
Pass 3	*Inlet*	-5.65	-5.28	-9.34	-6.14	-6.75	-6.77	-6.31	-6.08	-6.73	-6.92	-7.08	-6.09	-6.85	-6.56
	Outlet	0.50	1.83	-6.77	-2.10	-3.05	-3.13	-2.49	-2.38	-3.79	-3.72	-3.64	-3.84	-3.93	-3.66
Pass 4	*Inlet*	-10.21	-10.17	-17.76	-14.44	-14.86	-14.99	-14.71	-14.23	-15.23	-14.92	-14.96	-15.05	-15.18	-14.63
	Outlet	-1.52	-2.03	-4.72	-1.85	-2.68	-2.72	-2.38	-2.15	-2.74	-2.76	-2.76	-2.61	-2.99	-2.89
Pass 5	*Inlet*	-2.76	-2.87	-4.14	-1.81	-2.82	-2.76	-2.60	-2.34	-2.68	-2.74	-2.78	-2.42	-2.99	-2.84
	Outlet	0.26	0.35	-1.93	0.27	-0.43	-0.54	0.06	0.27	-0.50	-0.44	-0.46	-0.54	-0.62	-0.70
Pass 6	*Inlet*	-0.76	-0.69	-2.48	-0.31	-0.93	-1.07	-0.44	-0.25	-0.87	-0.80	-0.80	-0.84	-0.95	-0.97
	Outlet	0.26	0.46	-0.47	2.19	1.21	1.25	1.44	1.67	0.97	1.62	1.65	1.56	0.64	0.79
Average	*Inlet*	-3.40	-1.78	-8.31	-5.64	-6.15	-6.28	-6.01	-5.61	-6.77	-6.61	-6.59	-6.16	-6.57	-6.23
	Outlet	0.47	1.14	-5.04	-1.90	-2.56	-2.73	-2.43	-2.00	-3.19	-3.11	-3.27	-2.91	-3.45	-3.13
	Overall	-1.47	-0.32	-6.67	-3.77	-4.35	-4.51	-4.22	-3.81	-4.98	-4.86	-4.93	-4.54	-5.01	-4.68

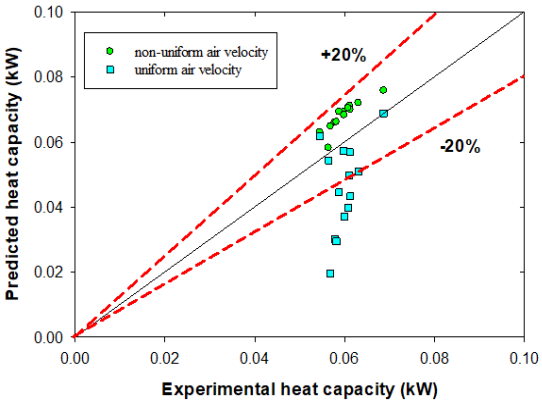

Figure 8. Comparison of the predicted and experimental heat capacities

The temperature of the refrigerant shows a sharp decrease in the first pass (0-0.3 m) in all data points according to Figure 9. In the first pass of the MCPH, decreases in temperature of the refrigerant are 10-12 ºC. In the second pass (0-0.7 m), reducing in the temperatures are lower than the decrease in the first pass owing to the decrement of the finite temperature difference between air and refrigerant. Therefore, the amount of the decreasing in refrigerant temperature declines as the refrigerant flows through the passes (lengths after 0.7 m). Under the considered operation condition, the test sample MCPH shows a higher temperature change in the first two passes. In the first and second passes, refrigerant temperatures have been nearly the same as the air temperature in the climate chamber. The high-temperature changes in first and second pass according to the changes in other passes indicate that the MCPH has been completed the great majority of the heat transfer duty in the first two passes

The heat transfer rates in each pass in terms of the length of the passes are depicted in Figure 10 for handled data points. It can be easily observed from the figure that the first pass shows the highest heat transfer rate among the passes of the MCPH. The heat transfer rate takes place in the second pass have been relatively higher than the heat transfer rate in the next passes under all investigated test conditions. In the next passes of the second pass, the heat transfer rate between air and refrigerant has slowly reduced and it closes to zero in the sixth pass (last pass of the MCPH). As mentioned above, the main reason for this situation is the decrement of the finite temperature difference between air and refrigerant through the length of the passes. It can be concluded that the temperature decrements and higher heat transfer rate in the first and second passes are the indicators of the compactness of the microchannel heat exchangers. The studies conducted by many researchers have always implied as a benefit that the microchannel heat exchangers are the compact design. According to the studies, the MCPHs show higher heat transfer performance in the small volumes. In this respect, the results of the model proposed in the current study indicate agreeable conclusion with the studies available in the literature.

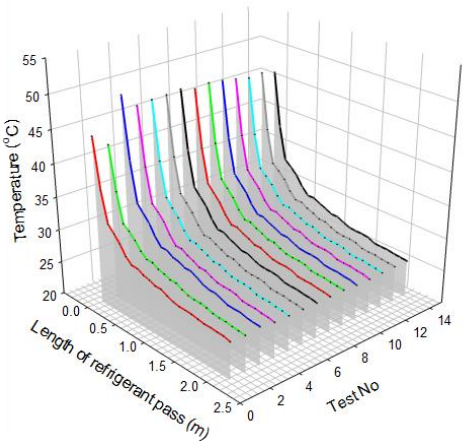

Figure 9. Temperature changes in passes of the MCPH with respect to the length of the refrigerant pass

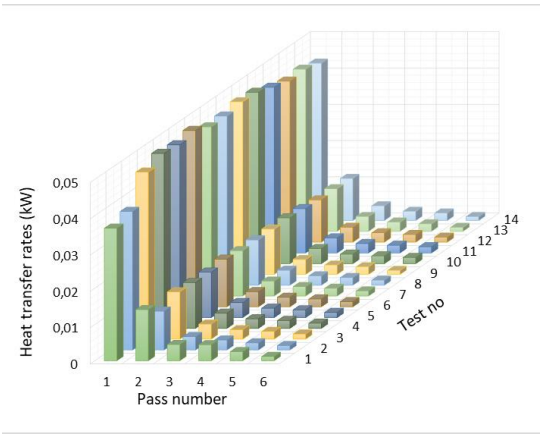

Figure 10. The heat transfer rates between air and refrigerant in passes of the MCPH for investigated test conditions.

4. Conclusion

The development of micro-manufacturing technologies has enabled the reveal of the microchannel heat exchangers for various industrial applications. It is well known that the single-phase conditions of the refrigerant are not widespread, whereas single-phase conditions are common in preheating and precooling, and in superheating and supercooling applications. Within this scope, the current study has presented a study on the prediction of the thermal performance of the louvered fin microchannel heat exchangers as air preheater for HVAC systems. A numerical model that uses the finite-volume approach including effectiveness-NTU procedure was introduced to estimate outlet temperature and heat capacity of the air-cooled microchannel heat exchanger. It is obvious that such simulation models can offer a significant contribution to the cost and time-saving design and optimization efforts of the designers owing to the elimination of the experimental tests. It is important to note here that the proposed model is also capable of simulating the heat transfer from air to the refrigerant even though heat transfer from the refrigerant to the air was considered in the tests conducted to verify the model.

During the simulation, it is observed that the estimations of the model have been in good agreement with experimental data regarding outlet temperature. It is determined that the model has reasonably predicted the outlet temperature of the MCPH with the mean absolute error deviation within 2%. The proposed model shows high accuracy with respect to temperature calculation. On the other hand, the model has indicated a higher deviation in the heat capacity prediction than the temperature estimation. It is concluded that the main reason for the high deviation in heat capacity prediction is the assumption which is neglect of the heat loss in the headers. The model applies the adiabatic header assumption but in the actual process, there is heat transfer from headers to ambient air. Therefore, it is considered that such heat transfer has an impact on heat capacity calculations. It is recommended that it should be taken into account during further simulation studies.

When comparing the results of heat capacity predictions of non-uniform air-side conditions with uniform ones, it has been apparently seen that applying non-uniform air side velocity with generating independent air-side grid regions improves the accuracy of the model. Considering different air velocities in terms of the actual configuration of the preheaters, especially fan-driven systems, have an important effect on the accuracy of the model.

Declaration

The author(s) declared no potential conflicts of interest with respect to the research, authorship, and/or publication of this article. The author(s) also declared that this article is original, was prepared in accordance with international publication and research ethics, and ethical committee permission or any special permission is not required.

Nomenclature

A_a	air-side overall heat transfer area (m^2)
A_f	fin surface area (m^2)
A_r	refrigerant side effective heat transfer area (m^2)
$\dot{Q}$	heat transfer rate (kW)
NTU	number of transfer units
C_R	heat capacity ratio (-)
C	heat capacity rate ($J\ K^{-1}\ s^{-1}$)
C_p	specific heat ($J\ kg^{-1}\ K^{-1}$)
D_h	tube hydraulic diameter (m)
f	friction factor (-)
F_d	fin width (m)
F_h	fin height (m)
F_p	fin pitch (m)
G	mass flux ($kg\ m^{-2}\ s^{-1}$)
h	heat transfer coefficient ($W\ m^{-2}\ K^{-1}$)
i	specific enthalpy ($kJ\ kg^{-1}$)
j	Colburn-j factor (-)
k_{tube}	thermal conductivity of tube material ($Wm^{-1}K^{-1}$)
k_{fin}	thermal conductivity of fin material ($W\ m^{-1}\ K^{-1}$)
L_l	louver length (m)
L_p	louver pitch (m)
L_{seg}	the segment length (m)
$\dot{m}$	mass flow rate ($kg\ s^{-1}$)
MAE	mean absolute error (%)
NTU	number of transfer units
Nu	Nusselt number (-)
Nu_{GN}	Gnielinski Nusselt number (-)
P	pressure (bar)
ΔP	pressure drop (bar)
Pr	Prandtl number (-)
P_t	port thickness (m)
$\dot{Q}$	heat transfer rate (kW)
Re_D	refrigerant side Reynolds number (-)
Re_{LP}	air-side Reynolds number (-)
T	temperature (ºC)
ΔT	temperature change (ºC)
T_{hi}	inner tube height (m)
T_p	tube pitch (m)

UA	overall heat transfer coefficient (kW K^{-1})
Um	mean velocity (m^{-1} s^{-1})
W_t	web thickness (m)
δ	fin thickness (m)
ρ	density (kg m^{-3})
ε	effectiveness (-)
η_o	overall fin efficiency (-)
η_f	fin efficiency (-)
η_{web}	web efficiency (-)
μ	dynamic viscosity (Pa.s)
θ	louver angle (^{o})
max	maximum
min	minimum
r	refrigerant
a	air
in	inlet
out	outlet

References

1. Sen, O., Yılmaz, C., *Thermodynamic performance analysis of geothermal and solar energy assisted power generation and residential cooling system*. International Advanced Researches and Engineering Journal, 2020. **04**(01): p.41–7.
2. Kandlikar, S.G., *A roadmap for implementing minichannels in refrigeration and air-conditioning systems - Current status and future directions*. Heat Transfer Enginering, 2007. **28**(12): p.973–85.
3. Roth, K., Westphalen, D., Dieckmann, J., Hamilton, S., Goetzler, W., *Energy consumption characteristics of commercial building HVAC systems*, Volume III: Energy savings potential, 2002. **3**.
4. Kandlikar, S.G., Garimella, S., Li, D., Stephane, C., King, M.R., *Heat transfer and fluid flow in minichannels and microchannels*. 2005, Oxford: UK: Elsevier.
5. Gong, L., Lu, H., Li, H., Xu, M., *Parametric numerical study of the flow and heat transfer in a dimpled wavy microchannel*. Heat Transf Research, 2016. **47(2)**: p.105–18.
6. Kaya, H., Ekiciler, R., Arslan, K., *Entropy generation analysis of forced convection flow in a semicircular microchannel with TiO2/water nanofluid*. Heat Transf Research, 2019. **50**(4): p.335–48.
7. Mohammadpourfard, M., Zonouzi, S.A., Mohseni, F., *Numerical study of the hydrothermal behavior and exergy destruction of magnetic nanofluid in curved rectangular microchannels*. Heat Transf Research, 2015. **46**(9): p.795–818.
8. Tiwari, N., Moharana, M.K., *Numerical study of thermal enhancement in modified raccoon microchannels*. Heat Transf Research, 2019. **50**(6): p.519–43.
9. Glazar, V., Frankovic, B., Trp, A., *Experimental and numerical study of the compact heat exchanger with different microchannel shapes*. International Journal of Refrigeration, 2015. **51**: p. 144–53.
10. Ren, T., Ding, G., Wang, T., Hu, H., *A general three-dimensional simulation approach for micro-channel heat exchanger based on graph theory*. Applied Thermal Engineering, 2013. **59**(1–2): p.660–74.
11. Yin, J.M., Bullard, C.W., Hrnjak, P.S., *R-744 gas cooler model development and validation*. Int J Refrig. 2001. **24**: 692–701.
12. Fronk, B.M., Garimella, S., *Water-coupled carbon dioxide microchannel gas cooler for heat pump water heaters: Part II - Model development and validation*. International Journal of Refrigeration, 2011. **34**(1): p.17–28.
13. Fronk, B.M., Garimella, S., *Water-coupled carbon dioxide microchannel gas cooler for heat pump water heaters: Part I - Experiments*. International Journal of Refrigeration, 2011. **34**(1): p.7–16.
14. García-Cascales, J.R., Vera-García, F., Gonzálvez-Maciá, J., Corberán-Salvador, J.M., Johnson, M.W., Kohler, G.T. *Compact heat exchangers modeling: Condensation*. International Journal of Refrigeration, 2010. **33**(1): p.135–47.
15. Kim, M.H., Bullard, C.W., *Development of a microchannel evaporator model for a CO2air-conditioning system*. Energy,. 2001. **26**(10): p.931–48.
16. Yin, X.W., Wang, W., Patnaik, V., Zhou, J.S., Huang, X.C., *Evaluation of microchannel condenser characteristics by numerical simulation*. International Journal of Refrigeration, 2015. **54**: p. 126–41.
17. Park, C.Y., Hrnjak, P., *Experimental and numerical study on microchannel and round-tube condensers in a R410A residential air-conditioning system*. International Journal of Refrigeration, 2008. **31**(5): p. 822–31.
18. Liang, Y.Y., Liu, C.C., Li, C.Z., Chen, J,P.. *Experimental and simulation study on the air side thermal hydraulic performance of automotive heat exchangers*. Applied Thermal Engineering, 2015. **87**: p.305–15.
19. Zhai, R., Yang, Z., Zhang, Y., Lv, Z., Feng, B., *Effect of temperature and humidity on the flammability limits of hydrocarbons*. Fuel, 2020. **270**. Available from: https://doi.org/10.1016/j.fuel.2020.117442
20. Ahmadpour, M.M., Akhavan-Behabadi, M.A., Sajadi, B., Salehi-Kohestani, A., *Experimental Study of Lubricating Oil Effect on R600a Condensation inside Micro-Fin Tubes*. Heat Transfer Engineering. 2020. p.1–13. Available from: https://doi.org/10.1080/01457632.2020.1735780
21. American Society of Heating R and AE. *ASHRAE Handbook-Fundamentals*. 2009, Atlanta, GA: ASHRAE Inc.
22. Lohbeck, W., *Development and state of conversion to hydrocarbon technology*. Proceedings of the International Conference on Ozone Protection Technologies: Washington, D.C.; 1996. p. 247–51.
23. Bergman, T.L., Lavine, A.S., Incropera FP, DeWitt DP. *Fundamentals ofHeat and Mass Transfer*. 7th ed. 2011, New York: USA: JohnWiley & Sons.
24. Cengel, Y.A., *Heat and Mass Transfer: A Practical Approach*. 3rd ed. 2007, McGraw-Hill.
25. Kuppan, T., *Heat Exchanger Desing Handbook*. 2000, NY: USA: Marcel Dekker, Inc.
26. Shah, R.K., Sekulic, D.P., *Fundamentals of Heat Exchanger Design*. 2003, New York: USA: John Wiley and Sons, Inc.
27. Kakaç, S., Liu, H., *Heat Exchangers: Selection, Rating and Thermal Design*. 2nd ed. 2002, Boca Raton, USA: CRC Press LLC.
28. Singh, V., Aute, V., Radermacher, R., *Numerical approach for modeling air-to-refrigerant fin-and-tube heat exchanger with tube-to-tube heat transfer*. Int J Refrig [Internet]. 2008. **31(8)**:1414–25.
29. Asinari, P., Cecchinato, L., Fornasieri. E., *Effects of thermal conduction in microchannel gas coolers for carbon dioxide*. International Journal of Refrigeration, 2004. **27**(6): p. 577–86.

30. Dittus, F.W., Boelter, L.M., *Heat transfer in automobile radiators of the tubular type*. Publication in Engineering University California, Berkeley. 1930. **2**: p.443.
31. Gnielinski, V., *New equations for heat and mass transfer in turbulent pipe and channel flow*. International Chemical Engineering, 1976.**16:** p.359–68.
32. Petukhov, B.S., *Heat transfer and friction in turbulent pipe flow with variable physical properties*. Advanced Heat Transfer, 1970. **6**: p.503–64.
33. Derby, M., Lee, H.J., Peles, Y., Jensen, M.K., *Condensation heat transfer in square, triangular, and semi-circular mini-channels*. International Journal of Heat and Mass Transfer, 2012. **55**(1–3): p.187–97.
34. Saha, S.K., *Microchannel Phase Change Transport Phenomena*. 2016, Oxford: UK: Butterworth-Heinemann.
35. Filonenko, G.K., *Hydraulic resistance in pipes", Heat Exchanger Design Handbook*. Teploenergetica, 1954. **1(4):** p.40–44.
36. Adams, T.M., Jeter, S.M., Qureshis, Z.H., *An experimental investigation of single-phase forced convection in microchannels*. International Journal of Heat and Mass Transfer, 1997. **41**(6–7): p.851–7.
37. Aute, V., Radermacher, R., *Chapter Five - A Validated Framework for Innovation and Design Optimization of Air-to-Refrigerant Heat Exchangers*. In: Sparrow EM, Abraham JP, Gorman JMBT-A in HT, Elsevier, 2018. p. 301–32.
38. Chang, Y.J, Wang, C.C., *A generalized heat transfer correlation for Iouver fin geometry*. International Journal of Heat and Mass Transfer, 1997. **40(3)**: p.533–44.
39. Kim, M., Bullard, C.W., *Air-side thermal hydraulic performance of multi-louvered fin aluminum heat exchangers*. International Journal of Refrigeration, 2002. **25**: p.390–400.
40. Klein, S.A., *Engineering Equation Solver, F-Chart Software*. 2006.